JOURNAL OF AIRCRAFT
Vol. 42, No. 2, March–April 2005

In-Flight Wing Deformation Characteristics During Limit-Cycle Oscillations

Charles M. Denegri, Jr.,* James A. Dubben,† and Daniel L. Maxwell‡
U.S. Air Force SEEK EAGLE Office, Eglin Air Force Base, Florida 32542-6865

Oscillatory wing response data were measured on an F-16C aircraft during limit-cycle-oscillation (LCO) testing of an external store configuration. The configuration tested exhibited typical LCO response in the transonic flight regime. Deformation characteristics were measured at 11 locations on the wing and missile launchers during various LCO events. These measurements allowed viewing of the aeroelastic mode of instability for various flight conditions. Details of a linear flutter analysis model are presented, and the predicted eigenmode from the linear flutter analysis is compared to the in-flight measured mode. The measured LCO modes are also compared for level flight vs elevated load factor flight and subcritical LCO vs critical LCO conditions. At the onset of LCO, the mode shape bears a strong resemblance to the flutter mode predicted by linear flutter analysis. Further, the wing deformation characteristics during LCO vary significantly with respect to Mach number and load factor. The nonsynchronous motion of the LCO diminishes and becomes more synchronous as the Mach number increases beyond 0.90. This contradicts the trends predicted by linear flutter analyses and suggests that a change in the oscillation bounding mechanism occurs over the flight region examined.

Nomenclature

f_f	=	linear analysis flutter frequency, Hz
f_n	=	natural frequency, Hz
$\hat{M}$	=	generalized modal mass
M_∞	=	freestream Mach number
V_f	=	linear analysis flutter velocity, knots true airspeed
α	=	intersection point; location where the deflected wingtip intersects the undeflected wingtip midplane
η	=	fraction of semispan

Introduction

THE understanding of the physical aeroelastic mechanisms that lead to limit-cycle oscillations (LCO) has been a topic of much research in recent years. These oscillations have been a recurring problem on certain fighter aircraft and are generally encountered on external store configurations that are theoretically predicted to be flutter sensitive. These sensitivities are quite evident during flight and are often the subject of extensive examination during flutter flight tests of aircraft that exhibit this behavior. Reference 1 provides a detailed description of the LCO phenomenon and its relationship to classical flutter. An excellent overview of LCO of fighter aircraft carrying external stores and its sensitivity to the store carriage configuration and mass properties is given in Ref. 2. These papers describe LCO as a phenomenon characterized by sustained periodic oscillations that neither increase nor decrease in amplitude over time for a given flight condition. These papers also describe the problems associated with this phenomenon and the elusiveness of predicting its occurrence theoretically.

LCO arises from the nonlinear interaction of the structural and aerodynamic forces acting on the affected aircraft component. It has long been speculated that LCO is a form of classical flutter, which is characterized by catastrophically diverging oscillations. But LCO differs from classical flutter in its tendency toward limited amplitude oscillations rather than diverging oscillations. The notion that LCO is a form of classical flutter is substantiated by the fact that the occurrence of LCO is usually associated with aircraft/store configurations that are predicted by linear analysis to be flutter sensitive.

In recent years, several approaches have been investigated for predicting the occurrence of LCO for fighter aircraft.[3–11] Because typical flutter and LCO analyses only give an indication of the potential in-flight behavior, flight testing of the most critical configurations is accomplished in order to verify the analyses and to determine the true LCO characteristics. Flight testing continues to become more and more expensive, while the number and combinations of store configurations are continually increasing. Hence, it is important to find methods that accurately determine the flutter and LCO characteristics of potentially dangerous configurations without the need for testing. It is equally desirable to identify those configurations whose response characteristics are acceptable and thereby eliminate the need for unnecessary testing.

In subsequent sections, wing deformation characteristics of a fighter aircraft with external stores are examined for several limit-cycle oscillation conditions. Prior work[12,13] showed measured flight-test results for a single response location and discussed various LCO characteristics. The present work shows measured deflections for several locations on the wing and missile launchers during various LCO events. These data provide qualitative insight into the actual physical mechanism involved in LCO as well as a quantitative comparison of the wing-tip motion characteristics predicted by analysis and observed during flight.

Flight Test

A brief discussion of the test aircraft, instrumentation, test methods, store configuration, store mass properties, and general flight-test results is presented in this section. A complete overview of Eglin Air Force Base flutter testing can be found in Refs. 13 and 14.

Test Aircraft

The aircraft used for this test was an F-16C, tail number 88-0441. This aircraft is a Block 40 F-16 modified for flutter testing. These

Received 21 March 2003; presented as Paper 2003-1426 at the AIAA/ASME/ASCE/AHS 44th Structures, Structural Dynamics, and Materials Conference, AIAA/ASME/AHS 11th Adaptive Structures Conference, AIAA 5th Non-Deterministic Approaches Forum, AIAA 4th Gossamer Spacecraft Forum, AIAA Dynamics Specialists Conference, Norfolk, VA, 7–11 April 2003; revision received 28 April 2004; accepted for publication 29 April 2004.

*Lead Flutter Engineer, Engineering Division, 205 West D Avenue, Suite 348. Senior Member AIAA.

†Lead Flutter Flight Test Engineer, Engineering Division, 205 West D Avenue, Suite 348. Member AIAA.

‡Senior Engineer, Avionics Test and Analysis Corporation, 205 West D Avenue, Suite 348. Member AIAA.

modifications made it uniquely capable of sensing, recording, and transmitting data gathered during aircraft flutter testing. The F-16 wing is a cropped delta planform blended with the fuselage and is composed of a NACA 64A-204 airfoil with a wing span of 30 ft. The wing aspect ratio is 3.0 and has a leading-edge sweep angle of 40 deg. Extra fuel can be carried in external tanks under the wings and the fuselage, and additional stores of various types can be carried on the wing tips, six wing stations, and one fuselage centerline station.

Instrumentation

The wing LCO response data were measured using accelerometers located on the forward and aft ends of the wing tip and underwing missile launchers and at the pylon-to-wing interface of the underwing store carriage stations. The forward launcher accelerometers were located approximately 4 in. aft of the launcher nose, and the aft accelerometers were located approximately 12 in. forward of the launcher tail.[14] The accelerometers in the pylons were located on the uppermost load-carrying structure nearest the pylon-wing interface. Details on the accelerometer locations are presented in Fig. 1 and Table 1. The measurement range of these accelerometers was $\pm 10g$ with a nominal sensitivity of 10 mv/g (at 100 Hz) and a noise floor of 0.0012 g (rms). Data were acquired at 325 sample/s using the Advanced Airborne Test Instrumentation System. Control surface position and basic aircraft flight parameters such as Mach number, altitude, and load factor (normal g) were also measured and transmitted via time-correlated signals to a ground receiver station in pulse-coded-modulation format.

Table 1 Accelerometer locations[a]

Station	Location	ID	x, in.	y, in.	z, in.
1	Wing-tip launcher	1 forward	318.0	183.0	91.0
		2 middle	378.0	183.0	93.0
		3 aft	403.0	183.0	96.0
2	Underwing launcher	4 forward	308.0	157.0	76.0
		5 aft	392.0	157.0	80.0
2	Pylon-wing interface	6 forward	368.3	156.3	91.3
		7 aft	385.2	157.0	92.0
3	Pylon-wing interface	8 forward	343.8	117.6	90.2
		9 aft	375.3	119.8	91.6
4	Pylon-wing interface	10 forward	309.9	71.0	89.5
		11 aft	376.9	71.0	90.5

[a]Left wing. Right wing locations are mirror image of the left wing.

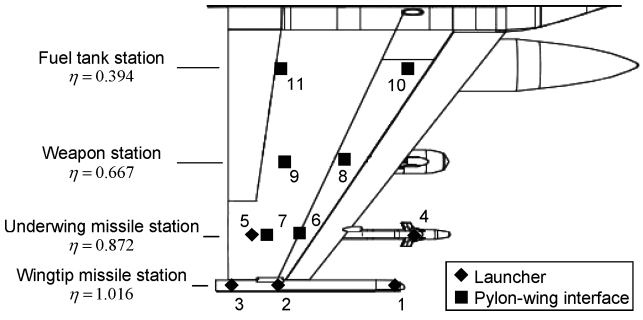

Fig. 1 Accelerometer locations (wing planform layout).

Test Methods

Testing began at 10,000-ft pressure altitude (altimeter setting of 29.92 in. Hg), and all test points were generally completed at that altitude before proceeding to another altitude. An onboard excitation system was used to determine the flutter sensitivity at the 10,000-, 5000-, and 2000-ft test points. Elevated load factor turns were also examined to determine the LCO sensitivity to these maneuvers. A test point maneuver was terminated when the response amplitude either exceeded predetermined termination criteria, or the response amplitude increased at such a rate as to rapidly approach the predetermined termination criteria.

General Flight-Test Results

Typical LCO is characterized by the gradual onset of sustained limited-amplitude wing oscillations, where the oscillation amplitude progressively increases with increasing Mach number and dynamic pressure.[13] The aircraft stores configuration examined here exhibited typical LCO characteristics. The store configuration is shown in Fig. 2. The store attachment reference points are given in Table 2, and the store mass properties are presented in Table 3. The maximum wing response levels for each test point in straight-and-level and elevated load factor flight are plotted with respect to Mach number and test altitude and are shown in Figs. 3 and 4. These data are from the forward wing-tip launcher accelerometer.

In level flight (Fig. 3), measurable oscillations were present from 0.70 to 0.95 Mach. At the 10,000-, 5000-, and 2000-ft test altitudes,

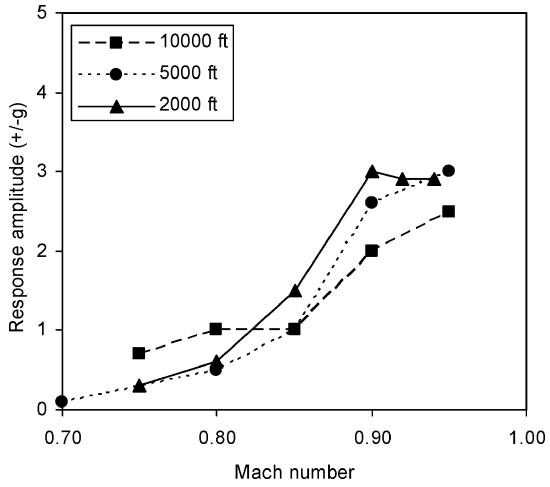

Fig. 3 Measured maximum oscillatory wing-tip response during level flight (forward vertical accelerometer).

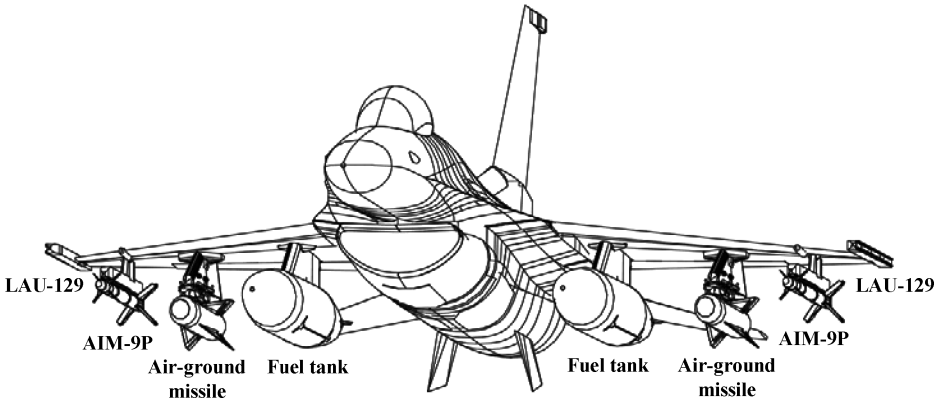

Fig. 2 External store configuration.

Table 2 Store configuration and attachment reference points

Station[a]	Location	x, in.	y, in.	z, in.	Store	Suspension equipment
1	Wingtip	380.46	180.00	92.00	None	LAU-129/A launcher
2	Underwing	371.56	157.00	91.35	AIM-9P missile	LAU-129/A launcher
3	Underwing	349.67	120.00	90.72	Air-ground missile	Launcher/pylon
4	Underwing	316.87	71.00	90.02	Empty 370-gallon fuel tank	Fuel tank pylon

[a]Left-wing station loading. For the flight test, the right wing was configured as a mirror image of the left wing (see Fig. 2).

Table 3 Store mass properties

		Center of gravity[a]			Moments of inertia, slug-ft.^{2}		
Store	Weight, lb	x, in.	y, in.	z, in.	Roll	Pitch	Yaw
LAU-129/A wingtip launcher	84.9	−15.20	0.00	−0.01	——	13.73	13.70
AIM-9P missile, LAU-129/A underwing launcher, and missile pylon	276.3	−14.65	0.01	−13.30	1.31	68.63	67.77
Air-ground missile, launcher, and weapon pylon	898.7	−2.27	0.02	−20.72	19.72	134.74	116.95
370 gallon fuel tank (empty) and pylon	470.5	−1.85	−0.18	−10.00	——	197.93	187.64

[a]Positive values are aft, outboard, or above the store attachment reference point x-y-z locations (see Table 2).

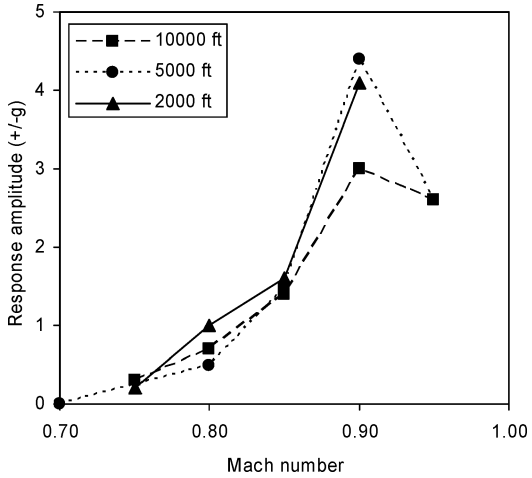

Fig. 4 Measured maximum oscillatory wing-tip response during elevated load factor flight (forward vertical accelerometer).

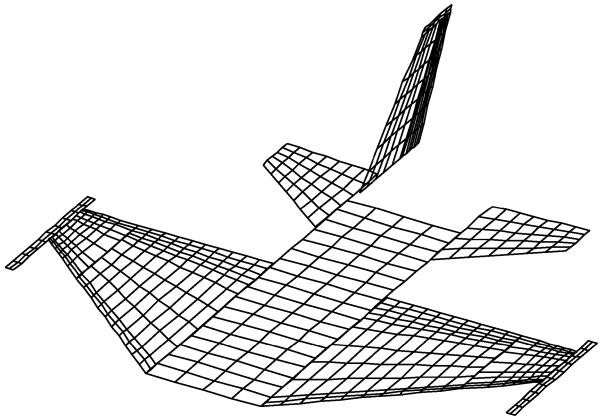

Fig. 5 Flutter-analysis doublet-lattice aerodynamic model.

the LCO amplitude increased somewhat exponentially with Mach number from initial onset up to 0.90 Mach. Above 0.90 Mach at all altitudes, the LCO amplitudes showed a trend of leveling off and remained relatively constant. For elevated load factor flight (Fig. 4), measurable oscillations were present from 0.75 to 0.95 Mach. At all three test altitudes, the oscillation amplitudes increased almost linearly from 0.75 to 0.85 Mach and showed a significant increase in amplitude at 0.90 Mach. At 0.95 Mach for the 10,000- and 5000-ft test altitudes, the LCO amplitude was lower than at 0.90 Mach. Elevated load factor flight was not investigated at 0.95 Mach, 2000 ft Overall, the dynamic aeroelastic characteristics of this configuration were well behaved and can be categorized as typical LCO. The instability response was antisymmetric and showed frequency variations from 7.9 to 8.2 Hz with the lowest frequencies seen at 0.90 Mach for all test altitudes.

Linear Flutter Analyses

Linear flutter analyses are accomplished for the flight-tested configuration to demonstrate the similarities between the measured wing deflections and those predicted by the linear analyses. Comparisons between the flight-test and linear-analysis results highlight the strengths and inadequacies of using these methods for predicting typical LCO. Velocity vs damping and velocity vs frequency plots, as well as the predicted flutter mode shape, are presented for the store configuration examined in this paper and are discussed in the following.

Linear flutter analyses are typically accomplished in the frequency domain and involve obtaining the natural vibration frequencies and modes, calculating the generalized aerodynamic forces, and then solving for the modal damping and frequency variations with velocity. This analysis assumes the response of the structure to be simple harmonic motion and is therefore limited to indicating the stability of particular modes with respect to flight velocity. The main shortcoming of linear flutter analysis methods with regard to LCO is that no indication of the oscillation amplitude is available. This parameter is of primary importance in the certification process because configurations that exhibit high-amplitude neutrally stable oscillations are typically avoided, whereas those exhibiting low-amplitude oscillations are typically deemed suitable for use. Even though linear flutter analyses are not capable of directly predicting LCO, these analyses have been shown to adequately identify LCO-sensitive store configurations and the oscillation frequency of the instability. Furthermore, prior studies[12,13] have shown that the modal composition of the LCO mechanism can be indicative of the general nature of the LCO sensitivities.

The full-span aircraft flutter analysis model is shown in Figs. 5 and 6. The model used for this work is not a specialized research flutter analysis model. This model is a typical industry flutter model used for high-volume flutter analysis associated with weapons certification. It is comprised of an aerodynamic model of the basic aircraft coupled with a dynamically representative model of the structure. The aerodynamic model (Fig. 5) is a doublet-lattice method[15] representation composed of 13 panels (inner wings, flaperons, outer wings, wing-tip launchers, fuselage, horizontal tails, vertical tail, and rudder) that are subdivided into 616 discrete boxes. No aerodynamic modeling of the underwing stores is included. The only influence of the underwing stores considered in the flutter analyses is their effect on the structural modal characteristics (i.e., mode shapes and frequencies). A finite element model composed of 8532 degrees of

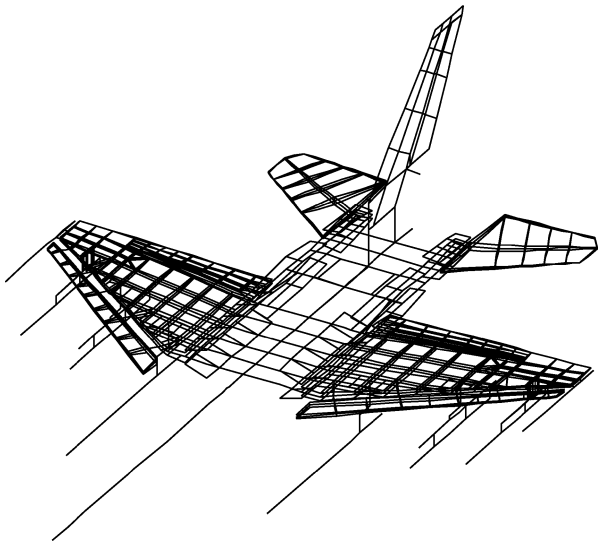

Fig. 6 Flutter-analysis finite element model.

freedom represents the aircraft structure, underwing stores, pylons, and launchers. The free-vibration analyses are performed using the Lanczos method of eigenvalue extraction. By considering only the modal deflections that influence the aerodynamic model, the system reduces to 252 structural points. Aerodynamic influence coefficients are computed for a range of Mach numbers, reduced frequencies, and air densities. The aerodynamic panels are splined to the vibration modes using the method of Harder and Desmarais.[16] The flutter equations are solved using the classical k-method of flutter solution. All flexible modes up to 25 Hz were retained for the flutter analyses. These modes included all fundamental wing modes and several store modes. Both symmetric and antisymmetric modes were included in the analyses because a full-span aircraft flutter model was used.

The analytical flutter speed is considered to be the velocity at which the modal damping curve of the known aeroelastically sensitive mode for the particular configuration crosses from stable to unstable (0% damping). It is considered to be directly comparable to the lowest airspeed at which self-sustained oscillations are encountered in flight.

To determine the theoretical flutter-sensitive mode and its stability characteristics, the linear flutter analyses presented in this section are accomplished using a nominal worst-case aerodynamic condition, specifically, sea-level air density at 0.90 Mach number. (Detailed matched-condition analyses will be presented in a subsequent section.) The flutter analysis results for the flight-tested configuration are presented in Fig. 7 and show a flutter speed of 493 knots true airspeed (KTAS) at 8.45 Hz for the outboard wing torsion mode (Fig. 8), which is coupled with the aft wing bending mode (Fig. 9). The damping curve for the flutter mode shows a moderately steep slope and crosses the 1% damping level at 540 KTAS. The flutter analyses indicate the flutter critical mode to be moderately sensitive to changes in airspeed and thus show good correlation to the flight-test data for velocity sensitivity, but there is no consistent correlation to the rate of oscillation amplitude increase. The predicted flutter frequency shows good correlation to the flight-test frequency, which ranged from 7.9 to 8.2 Hz.

The predicted flutter mode (complex eigenmode) from the linear flutter analysis is shown in Fig. 10 as superimposed snapshots at 36-deg phase increments for one oscillation cycle. The numerical sequence of the phase increment snapshots is annotated at the left of the figure near the aft end of the wing-tip launcher. The wing mode shape depicted in Fig. 10 shows the deformations predicted by the linear flutter analysis at the locations of the flight-test accelerometers (for the wing and tip launcher). Connection of the wing deformation locations sketches an outline that proceeds along the inboard fuel tank station chord line ($\eta = 0.394$), across the forward wing spar, down the outboard missile station chord line ($\eta = 0.872$), and then along the aft wing spar. This wing outline coincides closely with

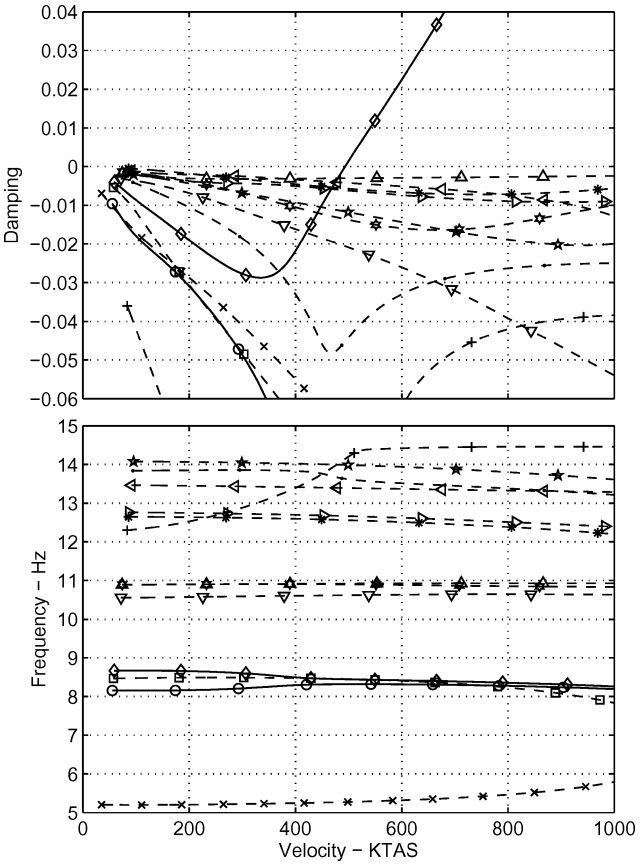

Fig. 7 Flutter analyses: $M_\infty = 0.90$, sea level, $V_f = 493.6$ KTAS, and $f_f = 8.45$ Hz.

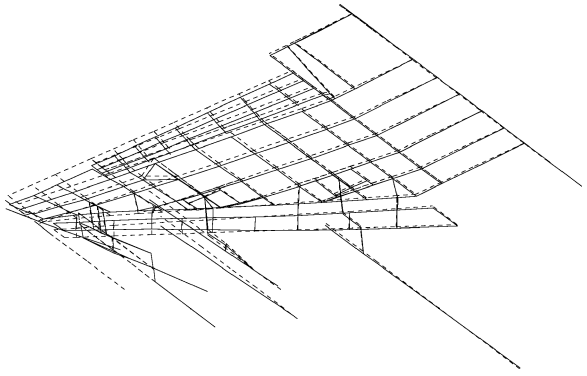

Fig. 8 Linear flutter mechanism unstable mode, antisymmetric outboard wing torsion, (right wing from full-span model): $f_n = 8.67$ Hz, and $\hat{M} = 0.672$.

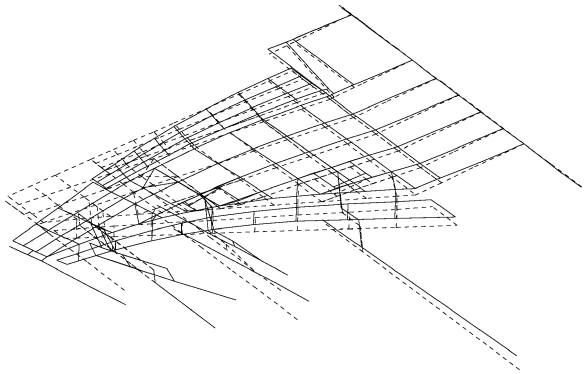

Fig. 9 Linear flutter mechanism coupled mode, antisymmetric aft wing bending (right wing from full-span model): $f_n = 8.16$ Hz, and $\hat{M} = 1.576$.

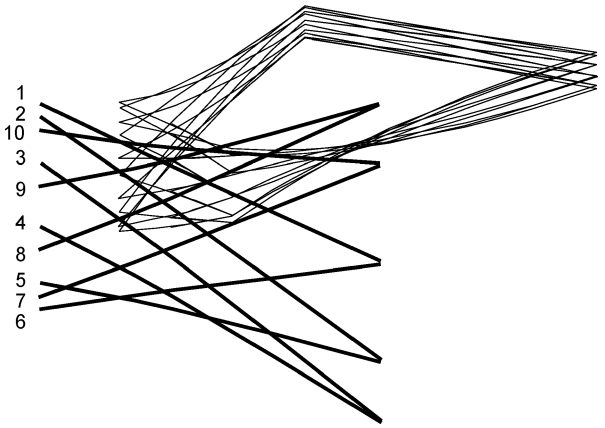

Fig. 10 Linear flutter analysis antisymmetric complex eigenmode: $M_\infty = 0.90$, sea level, $V_f = 493.6$ KTAS, and $f_f = 8.45$ Hz (right wing from full-span model, 36-deg phase increments).

that used to depict the flight-test wing deformation characteristics and minimizes visual clutter in the plot.

Examination of Fig. 10 shows that significant nonsynchronous motion is evident. The launcher nose leads the tail with the nose-down pitching motion nearly completed before the wing begins its downward plunge. There is a broad nodal region at the wing trailing edge extending from inboard to outboard of midspan and a very narrow nodal region at the wing leading edge slightly outboard of $\eta = 0.667$.

In the next section, comparisons between the linear predicted flutter mode shape and the LCO mode shapes measured in flight will be presented and discussed. Of particular interest is the similarity between the linear analysis results and the flight-measured mode shape at the onset of LCO.

Instability Mechanisms

Wing deformation characteristics were measured for an external store configuration that exhibited LCO in the transonic flight regime. Acceleration measurements from 11 locations on each wing and underwing launchers were acquired in both the vertical and lateral directions. The accelerometers at the middle location of the wing-tip launcher and the aft location of the station 3 pylon-wing interface malfunctioned during flight. The data from these accelerometers are omitted from the discussion presented in the following. Also, the underwing launcher data were omitted from the plots for ease of viewing the wing deformation characteristics.

A sample of the measured time histories from seven of the vertical-direction accelerometers is shown in Fig. 11. Composite plots of these response measurements superimposed at their respective spatial locations are shown in Figs. 12a–12f. Similar to the predicted flutter mode from linear analysis, these figures show the measured LCO modes as superimposed snapshots at 36-deg phase increments through one oscillation cycle. The numerical sequences of the phase-increment snapshots are annotated at the left of the figure near the aft wing-tip launcher accelerometer location. In each of these figures, the shape of the aeroelastic mode is quite evident.

Motivated by the results presented in Ref. 17, the measured LCO mode shapes have been analyzed for trends that would provide insight into the physical mechanisms that lead to LCO of fighter aircraft. Mode shapes for several Mach number, altitude, and load factor flight conditions are presented. Direct comparisons between measured mode shapes for level flight, elevated load factor flight, subcritical LCO conditions, and critical LCO conditions are presented, and the variations in the deformation characteristics are discussed.

In-flight wing deformation characteristics during LCO are presented for three Mach numbers (0.85, 0.90, and 0.95) at 5000 ft. The rationale for selecting these flight conditions follows. The test points at 5000-ft altitude were chosen because they showed response amplitudes nearly as high as the 2000-ft test points but had more

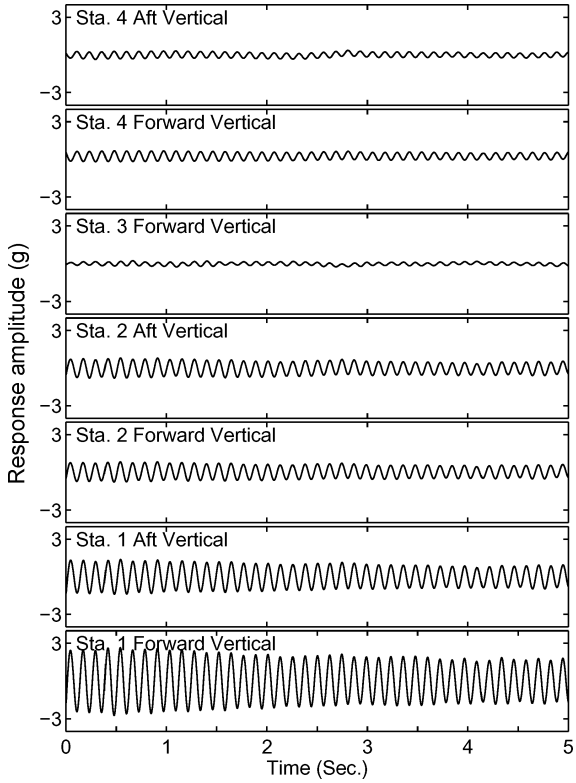

Fig. 11 Measured accelerometer response during LCO (0.95 Mach, 5000 ft, 2.7*g* load factor).

complete elevated load factor test data. The 0.85 Mach test point was chosen because it exhibited deformation characteristics that were essentially the same as the characteristics at the initial onset of LCO, which occurred at 0.75 Mach. Also, this test condition provides a convenient progression through the Mach region of interest. The 0.90 Mach test point was chosen because it represents the flight conditions where the LCO response exhibited a significant increase in amplitude. The 0.95 Mach test point was chosen because it showed the highest-amplitude LCO response at 5000 ft and also showed different deformation characteristics than the lower-Mach-number test points.

0.85 Mach, Level Flight

The measured LCO mode shape for 0.85 Mach at 5000 ft in level-flight is shown in Fig. 12a. The wing deformation characteristics at these flight conditions are essentially the same as those at the LCO onset conditions of 0.75 Mach. The oscillation cycle depicted was extracted during steady (nearly constant amplitude) LCO response prior to any artificial excitation from the onboard system. Significant nonsynchronous motion is present. The launcher nose leads the tail, and the nose-down pitching motion continues through the first half of the wing downward plunge. There is a broad aft nodal region centered near $\eta = 0.667$, a very narrow forward nodal region centered slightly inboard of this semispan location, and moderate outboard wing motion ($\eta = 0.872$) relative to the wing-tip launcher ($\eta = 1.106$). This mode is qualitatively very similar to the predicted linear flutter mode (Fig. 10). Two distinct differences are that the measured mode shows a forward nodal region that is farther inboard and the nose-down pitching motion of the wing-tip launcher continues through the first half of the wing downward plunge.

0.85 Mach, Elevated Load Factor Flight

Figure 12b shows the measured LCO mode shape for 0.85 Mach at 5000 ft during elevated load factor flight. The oscillation cycle depicted was extracted during steady LCO response while stabilized in a 2-*g* turn. Significant nonsynchronous motion is present. Similar to the level-flight response at these flight conditions, the launcher nose leads the tail, and the nose-down pitching motion continues

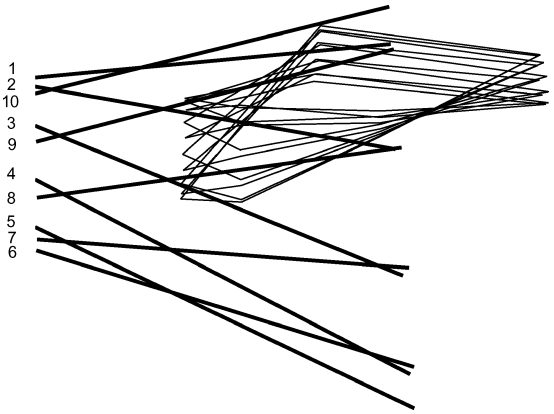

a) 0.85 Mach, level flight

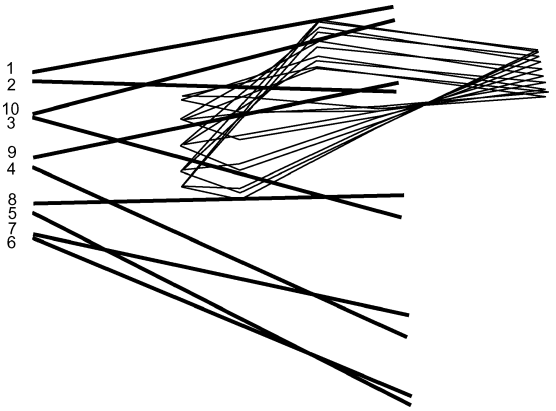

b) 0.85 Mach, 2-*g* load factor

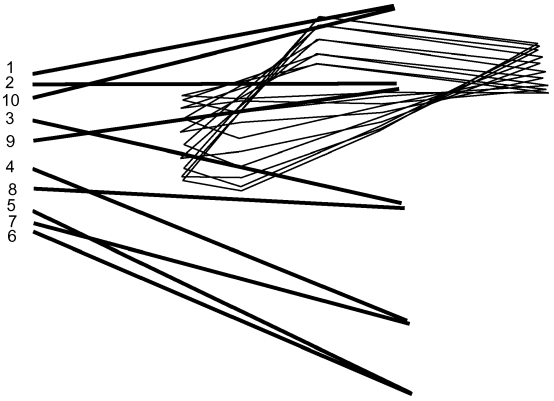

c) 0.90 Mach, level flight

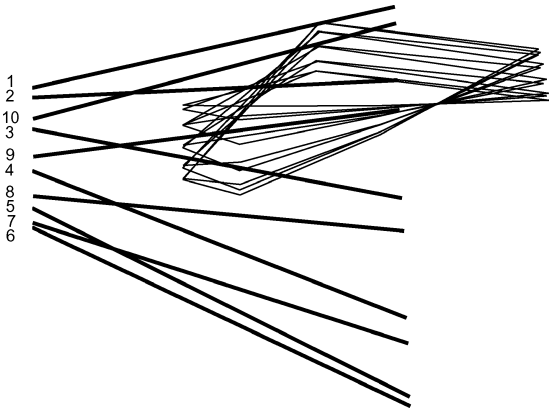

d) 0.90 Mach, 2.5-*g* load factor

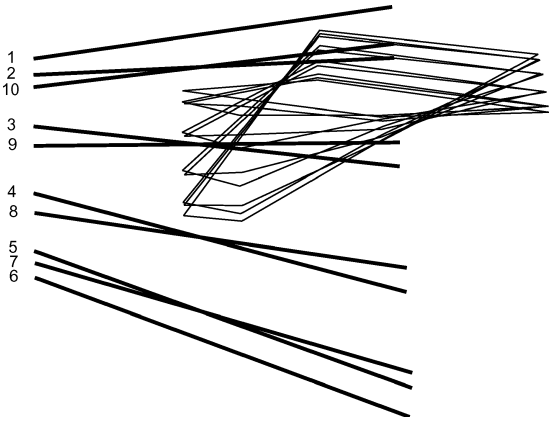

e) 0.95 Mach, level flight

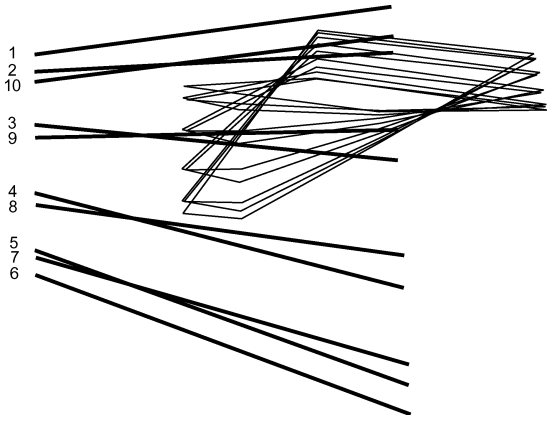

f) 0.95 Mach, 2.7-*g* load factor

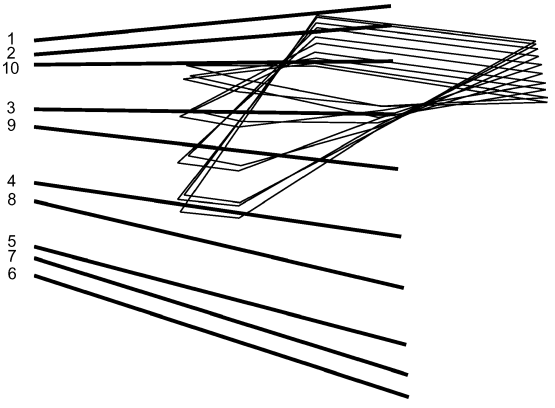

g) 0.95 Mach, 3.7-*g* load factor flight, diminishing LCO amplitude

Fig. 12 Measured LCO mode shapes, 5000-ft flight conditions (right wing, snapshots superimposed at 36-deg phase increments).

slightly farther than halfway through the wing downward plunge. Again, there is a broad aft nodal region centered near $\eta = 0.667$, but the forward node has essentially collapsed to a point centered slightly inboard of this semispan location. Moderate outboard wing motion ($\eta = 0.872$) relative to the wing-tip launcher ($\eta = 1.106$) is once again present.

0.90 Mach, Level Flight

The measured LCO mode shape for 0.90 Mach at 5000 ft in level-flight is shown in Fig. 12c. The wing deformation characteristics at these flight conditions showed a significant increase in amplitude from those seen at the previous flight conditions. The oscillation cycle depicted was extracted during steady LCO response after the effects of artificial excitation from the onboard system and prior to initiation of an elevated load factor maneuver. Moderate nonsynchronous motion is present, slightly less than for 0.85 Mach. The launcher nose continues to lead the tail through the oscillation cycle. Similar to the elevated load factor test condition during the previous test point, the nose-down pitching motion continues slightly farther than halfway through the wing downward plunge. The aft nodal region has narrowed somewhat but is still centered near $\eta = 0.667$. Similar to the level-flight condition at 0.85 Mach, there is a very narrow forward nodal region and moderate outboard wing motion at $\eta = 0.872$.

0.90 Mach, Elevated Load Factor Flight

Figure 12d shows the measured LCO mode shape for 0.90 Mach at 5000 ft during elevated load factor flight. The oscillation cycle depicted was extracted during a 2.5-g turn while the load factor was still increasing slightly. The LCO response amplitude was also increasing slightly. Moderate nonsynchronous motion is present similar to the level-flight response at these flight conditions. The launcher nose leads the tail, and the nose-down pitching motion again continues slightly farther than halfway through the wing downward plunge. Again, there is a narrow aft nodal region centered near $\eta = 0.667$, and similar to the elevated load factor condition at 0.85 Mach the forward node has essentially collapsed to a point. Moderate outboard wing motion ($\eta = 0.872$) relative to the wing-tip launcher is once again present but appears to be slightly less than at 0.85 Mach.

0.95 Mach, Level Flight

The measured LCO mode shape for 0.95 Mach at 5000 ft in level flight is shown in Fig. 12e. The wing deformation characteristics at these flight conditions showed the maximum amplitude response of all level flight-test points. The oscillation cycle depicted was extracted during steady LCO response prior to initiation of an elevated load factor maneuver. The wing motion is now nearly synchronous, but the launcher nose still slightly leads the tail through the oscillation cycle. The aft nodal region has narrowed to a point centered near $\eta = 0.667$. Similar to both previous level flight-test conditions, there is a very narrow forward nodal region but much larger outboard wing motion ($\eta = 0.872$) relative to the wing-tip launcher ($\eta = 1.106$).

0.95 Mach, Elevated Load Factor Flight

Figure 12f and 12g show the measured LCO mode shape for two different elevated load factors at 0.95 Mach at 5000 ft. The wing deformation characteristics at these flight conditions showed the maximum amplitude response of all test points. Figure 12f shows an oscillation cycle extracted during steady LCO while stabilized in a 2.7-g turn. Nearly synchronous motion is present similar to the level-flight response at these flight conditions. The launcher nose still slightly leads the tail through the oscillation cycle. The aft nodal region is extremely narrow but not quite a point as seen for the level-flight condition at this Mach number. It is still centered near $\eta = 0.667$, and the outboard wing motion relative to the wing-tip launcher ($\eta = 1.106$) is large. Consistent with the previous elevated load factor flight-test points, the forward node has essentially collapsed to a point centered slightly inboard of $\eta = 0.667$.

Figure 12g shows an oscillation cycle extracted during steady LCO while stabilized in a 3.7-g turn. Synchronous motion is present at these flight conditions. Further increases in load factor caused the LCO to cease. Similar to the level flight-test condition at this Mach number, the aft nodal region has narrowed to a point centered near $\eta = 0.667$, and the outboard wing motion relative to the wing-tip launcher is large. Also similar to the previous elevated load factor flight-test points, the forward node has collapsed to a point centered slightly inboard of $\eta = 0.667$.

Wing-Tip Motion Characterization

Three-dimensional snapshot views of the flight-measured mode shape deformations were shown for several flight conditions in the preceding section. In this section, a quantitative comparison of the wing-tip motion characteristics will be presented for both the flight-measured deformations and those predicted from linear flutter analysis. The deformation variations with respect to Mach number will be examined for the flight-test and linear-analysis data as well as the flight-test variations between level and elevated load factor flight.

Methodology

The natural mode shapes are important components for the prediction of in-flight LCO.[12,13] The wing node line in particular is a key indicator of LCO behavior. The two natural modes that combine to create the flutter mode are altered by their interaction with the aerodynamic forces so that at the flutter speed both have a similar galloping (nonsynchronous) character. The main difference lies in the fact that for the unstable flutter mode the wing is moving in a way that will extract energy from the airstream, whereas the stable coupled mode is being damped by the airstream.

The best way to visualize this behavior is to observe the modes in motion; however, it is clearly difficult to portray this dynamic motion in a static media. It is also difficult to compare several configurations directly because there are many characteristics of the mode shape that must be considered.

To make such a comparison more accessible, one can examine the motion of the wing tip as a representation of the complex mode shape.[18] This can be done by drawing a line between two points on the wing-tip launcher and extending it infinitely in both directions. The forward and aft accelerometer locations are convenient for this purpose and will be used here. This line through the launcher will intersect the imaginary extension of the undeflected launcher during a cycle of oscillation. The location where this line intersects the midplane of the undeflected wing-tip launcher is then defined as the intersection point α. The intersection point axis is defined as the imaginary line extending through the midplane of the undeflected launcher, where the aft-most point on the wing-tip launcher is located at 0 and the foremost point is located at 1. Values for α are not restricted to occur within the launcher chord and can range from $+\infty$ to $-\infty$. A deflected state that intersects midway between these locations would have an intersection point at 0.5. A horizontal wing-tip deflection state would have an intersection point at infinity (see Fig. 13 for an illustration of these examples).

The complex eigenvector provides both a displacement and a phase angle. Considering only vertical translations, if the two displacements are not in phase, that is, if they are nonsynchronous, then this point of intersection will move relative to the undeflected state as the wing progresses through an oscillation cycle. The intersection point movement can then be plotted with the abscissa as the oscillation cyclic angle and the ordinate as the location of the intersection point. A flat (horizontal) curve on this plot is indicative of synchronous motion.

Using the definitions just described for the intersection point, its axis, and its motion, all natural modes are thus represented as horizontal lines. Wing bending would be represented by a line at infinity, while wing torsion would be shown as a line between 0 and 1. For the F-16, wing bending does not typically result in a completely horizontal launcher position so the values are finite.

At nonzero airspeeds, the curves become more interesting (see Fig. 14). The asymptotes indicate that the wing-tip launcher has reached a horizontal position. The intersection curve repeats itself once during a single oscillation cycle of the wing (360 deg), tracing the same path during the upward motion of the wing as it does

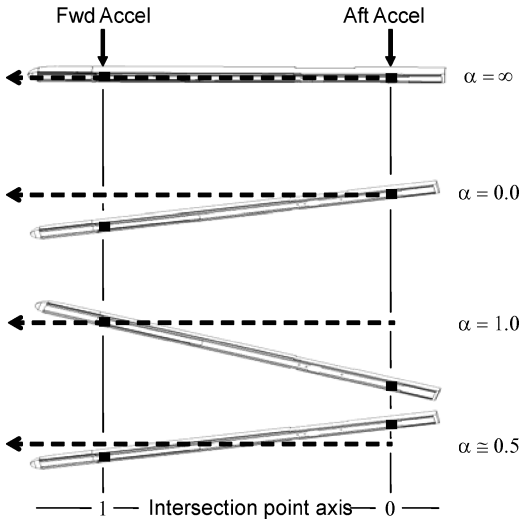

Fig. 13 Intersection point α.

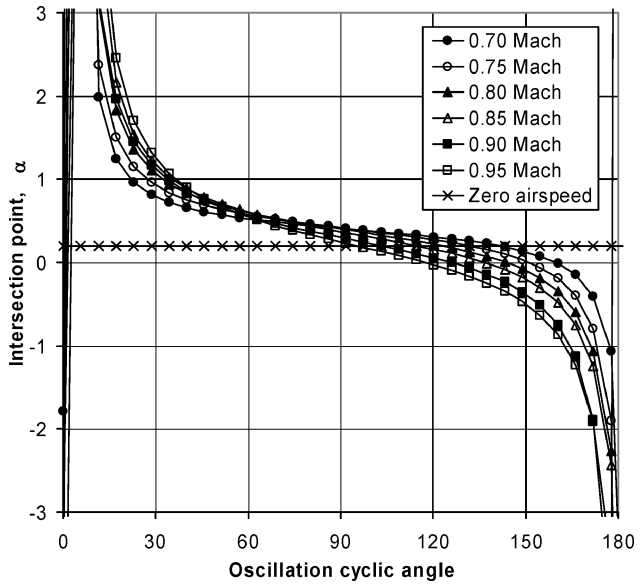

Fig. 14 Linear-flutter-analysis intersection point variation, unstable mode, 5000 ft, right wing-tip launcher.

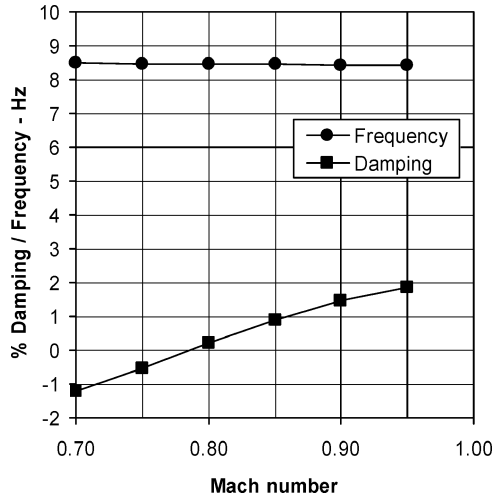

Fig. 15 Linear-flutter-analysis damping and frequency variation, 5000 ft, unstable mode.

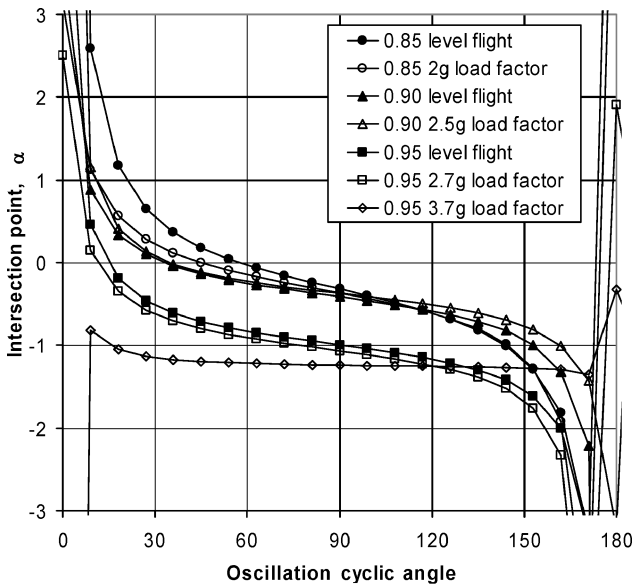

Fig. 16 Measured LCO intersection point variation, 5000 ft, right wing-tip launcher.

during the downward motion. For brevity, only the first half of the cycle is shown here. The slope of the nearly linear portion of the curve is indicative of the fluttering characteristic of the wing, with a negative slope indicating instability. Because the beginning of the oscillation cycle is arbitrarily defined, the plots are shifted such that the asymptotes representing a horizontal launcher position are aligned allowing for an easier visual comparison between the curves. For reference, the flat curve of a natural mode (i.e., zero airspeed mode) is also shown in Fig. 14.

Linear Flutter Analyses

The deformation of the critical flutter mode is examined for six Mach numbers at 5000-ft air density conditions. For these analyses, the density and Mach number are specified and held constant, and the critical mode is evaluated at the velocity that is consistent with these matched conditions. The deformation characteristics of the computed complex eigenmode are then examined as it transitions from stable to unstable in the vicinity of zero damping. The wing-tip intersection point characteristics for the critical mode are shown in Fig. 14, and the associated damping and frequency variations for these cases are shown in Fig. 15.

Two features are evident from the results shown in Fig. 14. First, the focus of the motion, that is, the mean intersection point over an oscillation quarter-cycle, moves aft on the launcher as Mach number increases. Second, the nearly linear portion of the curves show an increasingly negative slope as Mach number increases. The damping results (Fig. 15) show a fairly linear decrease in stabilizing damping for the critical mode as Mach number increases. Considering this trend in combination with the negative slope trend of the intersection point indicates that the critical mode becomes less synchronous as it becomes more unstable. This behavior is consistent with the underlying linear theory and is most likely a consequence of the linear assumptions necessary to perform the flutter analysis.

Flight Test

The wing-tip intersection point variations for the LCO flight-test cases presented earlier are evaluated in this section. These cases comprise three Mach numbers at 5000-ft altitude for both level and elevated load factor flight conditions.

The wing-tip intersection point characteristics for the measured LCO are shown in Fig. 16. The intersection point motion is generally shifted aft on the launcher compared to the linear flutter analyses shown in Fig. 14. As was seen in the linear analysis, the focus of the motion moves aft with increasing Mach number, but there is a much larger jump from 0.90 to 0.95 Mach for the flight test than was seen in the analysis. Contrary to the analytical results, however, the motion becomes more synchronous as Mach number increases.

The motion also becomes more synchronous with increasing load factor, and for the last case with diminishing LCO at 0.95 Mach and 3.7-*g* load factor, the intersection point curve is nearly flat, showing that the motion is virtually synchronous.

Conclusions

Oscillatory wing response data were measured on an F-16C aircraft during limit-cycle-oscillation (LCO) testing of an external store configuration. The configuration tested exhibited typical LCO response in the transonic flight regime. Deformation characteristics were measured at 11 locations on the wing and missile launchers during various LCO events. These measurements allowed for viewing the aeroelastic mode of instability for various flight conditions.

Variations in the deformation characteristics between the various flight conditions were evaluated to gain insight into the physical mechanism involved in the LCO response. In particular, the unstable mode shapes from three level-flight and four elevated load factor conditions were examined. These cases represented subcritical and critical LCO conditions. In addition, details of a linear-flutter-analysis model were presented, and the flutter mode (complex eigenmode) predicted by this analysis model was compared to the in-flight measured mode.

It has long been speculated that typical LCO encountered on fighter aircraft has its origins in classical flutter. This is based on the premise that linear flutter analysis results often correlate reasonably well to flight-test results, at least with respect to instability onset velocity and frequency. Substantial support for this notion is found in the cases presented here. The predicted velocity and frequency are within the range of the flight-test results. Further, it is observed that, at the onset of typical LCO, the mode shape bears a strong resemblance to the flutter mode. This implies that the fundamental instability mechanism is the same for both LCO and classical flutter. However, the similarities to classical flutter do not hold beyond initiation of the instability. Not only are the resulting oscillation amplitudes different (for classical flutter the oscillation amplitude is unbounded while for LCO the amplitude is limited by some unknown mechanism) but linear analyses show a trend toward greater nonsynchronous behavior as Mach number increases, whereas flight test shows the opposite trend.

Some insight into the nature of the oscillation amplitude bounding mechanism might be available from the observations of the wing deformation characteristics during LCO, which were seen to vary with respect to Mach number and load factor. Specifically, the aft nodal region was observed to narrow as Mach number increased for both level-flight and elevated load factor maneuvers. Conversely, the forward nodal region did not change as Mach number increased, but did narrow to a point for elevated load factors. Evidence from some researchers suggests that a wing at elevated load factors can exhibit stiffness characteristics more similar to a plate than a beam.[17] The variation of wing deformation characteristics seen here could be indicative of this type of behavior.

Related to these node variations is the nonsynchronous motion of the LCO, which is most readily seen at the wing-tip launcher. This motion was observed to diminish and become more synchronous as Mach number increased beyond 0.90. Further, at elevated load factors as the LCO was beginning to diminish in amplitude the motion was observed to become almost purely synchronous while still maintaining steady LCO. This behavior strongly suggests that a change in the driving mechanism occurred. The proximity of this behavior to the transonic Mach numbers could be an indicator of shock interactions with the fundamental aeroelastic instability.

These results suggest that different mechanisms exist for LCO in the subcritical state, that is, at the initial onset of LCO, vs in the critical state (when the oscillation amplitude is large or increasing rapidly with small changes in flight conditions). Further, the presence of different mode shapes for level flight vs elevated load factor flight implies that the underlying mechanism leading to LCO during these flight conditions also changes.

The data presented herein are useful for direct comparison to the modal deformations predicted by linear and nonlinear aeroelastic solvers. The time-varying deformations of several wing locations from the solution results can be superimposed to show the predicted wing deformation characteristics. Likewise, the wing-tip intersection point variations can be examined to determine the characteristics of the nonsynchronous (galloping) behavior of the wing. Qualitative and quantitative comparisons of the solution results to the flight-measured data in this fashion will ensure that the correct fundamental instability is being obtained from the theoretical solution. The presence of significantly different mode shapes from the analysis would be indicative of weaknesses or flaws in the theory or solution procedure.

To alleviate the need for extensive flight testing, a fundamental understanding of the mechanisms involved in LCO is required. Further, a nonlinear flutter analysis capability is required that is capable of accurately predicting the type of LCO response characteristics presented in this paper. In support of these goals, the data contained herein are presented as a realistic check case to further aid progress in the development and validation of nonlinear flutter-analysis theories and codes.

References

[1]Bunton, R. W., and Denegri, C. M., Jr., "Limit Cycle Oscillation Characteristics of Fighter Aircraft," *Journal of Aircraft*, Vol. 37, No. 5, 2000, pp. 916–918.

[2]Norton, W. J., "Limit Cycle Oscillation and Flight Flutter Testing," *21st Annual Symposium Proceedings*, Society of Flight Test Engineers, Lancaster, CA, 1990, pp. 3.4-1–3.4-12.

[3]Cunningham, A. M., Jr., and Meijer, J. J., "Semi-Empirical Unsteady Aerodynamics for Modeling Aircraft Limit Cycle Oscillations and Other Non-Linear Aeroelastic Problems," *Proceedings of the International Forum on Aeroelasticity and Structural Dynamics*, Vol. 2, Royal Aeronautical Society, London, 1995, pp. 74.1–74.14.

[4]Meijer, J. J., and Cunningham, A. M., Jr., "A Semi-Empirical Unsteady Nonlinear Aerodynamic Model to Predict Transonic LCO Characteristics of Fighter Aircraft," AIAA Paper 95-1340, April 1995.

[5]Chen, P. C., Sarhaddi, D., and Liu, D. D., "Limit-Cycle Oscillation Studies of a Fighter with External Stores," AIAA Paper 98-1727, April 1998.

[6]Denegri, C. M., Jr., and Johnson, M. R., "Limit Cycle Oscillation Prediction Using Artificial Neural Networks," *Journal of Guidance, Control, and Dynamics*, Vol. 24, No. 5, 2001, pp. 887–895.

[7]Johnson, M. R., and Denegri, C. M., Jr., "Comparison of Static and Dynamic Neural Networks for Limit Cycle Oscillation Prediction," *Journal of Aircraft*, Vol. 40, No. 1, 2003, pp. 194–203.

[8]Toth, R. G., Canfield, R. A., and Melville, R., "Nonlinear Transonic Flutter Analysis for F-16 Stores Configuration Clearance," AIAA Paper 2002-1212, April 2002.

[9]Chen, P. C., Sulaeman, E., Liu, D. D., and Denegri, C. M., Jr., "Influence of External Store Aerodynamics on Flutter/LCO of a Fighter Aircraft," AIAA Paper 2002-1410, April 2002.

[10]Melville, R., "Nonlinear Simulation of F-16 Aeroelastic Instability," AIAA Paper 2001-0570, Jan. 2001.

[11]Melville, R., "Nonlinear Mechanisms of Aeroelastic Instability for the F-16," AIAA Paper 2002-0817, Jan. 2002.

[12]Denegri, C. M., Jr., and Cutchins, M. A., "Evaluation of Classical Flutter Analyses for the Prediction of Limit Cycle Oscillations," AIAA Paper 97-1021, April 1997.

[13]Denegri, C. M., Jr., "Limit Cycle Oscillation Flight Test Results of a Fighter with External Stores," *Journal of Aircraft*, Vol. 37, No. 5, 2000, pp. 761–769.

[14]Dreyer, C. A., and Shoch, D. L., "F-16 Flutter Testing at Eglin Air Force Base," AIAA Paper 86-9819, April 1986.

[15]Albano, E., and Rodden, W. P., "A Doublet-Lattice Method for Calculating Lift Distributions on Oscillating Surfaces in Subsonic Flows," *AIAA Journal*, Vol. 7, No. 2, 1969, pp. 279–285.

[16]Harder, R. L., and Desmarais, R. N., "Interpolation Using Surface Splines," *Journal of Aircraft*, Vol. 9, No. 2, 1972, pp. 189–191.

[17]Tang, D., and Dowell, E. H., "Effects of Angle of Attack on Nonlinear Flutter of a Delta Wing," *AIAA Journal*, Vol. 39, No. 1, 2001, pp. 15–19.

[18]Maxwell, D. L., and Dawson, K. S., "Analytical Aeroelastic Characteristics of F-16 Asymmetric External Store Configurations," AIAA Paper 2004-1755, April 2004.